IEEE Access
Multidisciplinary | Rapid Review | Open Access Journal

Received December 2, 2019, accepted January 9, 2020, date of publication January 17, 2020, date of current version January 28, 2020.

Digital Object Identifier 10.1109/ACCESS.2020.2967474

Endoscopic Path Planning in Robot-Assisted Endoscopic Nasal Surgery

YUCHENG HE, PENG ZHANG, XIAOZHI QI, BAOLIANG ZHAO, SHIBO LI, AND YING HU, (Member, IEEE)

Shenzhen Key Laboratory of Minimally Invasive Surgical Robotics and System, Shenzhen Institutes of Advanced Technology, Chinese Academy of Sciences, Shenzhen 518055, China

Corresponding authors: Xiaozhi Qi (xz.qi@siat.ac.cn) and Ying Hu (ying.hu@siat.ac.cn)

This work was supported in part by the National Natural Science Foundation of China under Grant U1613224, Grant U1713221, and Grant U1813213, in part by the Key Fundamental Research Program of Shenzhen under Grant JCYJ20180507182415428 and Grant JCYJ20180507182215361, and in part by the Shenzhen Key Laboratory Project under Grant ZDSYS201707271637577.

ABSTRACT In robot-assisted endoscopic nasal surgery, due to the slender and complicated nasal cavity and sinus anatomical structure, the nasal endoscope of robot end-effector is prone to injure surrounding tissues during surgical approaches. In order to improve the movement safety of the endoscope in robot-assisted endoscopic nasal surgery, a path planning method for endoscopic surgical approaches based on medical image pixel map searching is proposed in this paper, and safe surgical paths from the nasal entrance point to the operating areas are obtained. Firstly, through the trajectory analysis of nasal endoscope tip during surgery, the path planning requirements of endoscope tip are analyzed and obtained. Then, considering the slender and complicated anatomy of the nasal cavity, a binarized three-dimensional grid map containing the spatial anatomy of the nasal cavity is constructed based on the patient's CT medical image sequence. The endoscopic surgical approaches are searched and optimized by introducing the A-star algorithm, and safe surgical paths from the nasal entrance point to the operating areas are obtained. Finally, a virtual nasal endoscopy system is developed and tested on a head model containing nasal tissue, and the effectiveness of the planned surgical paths is verified by automatic virtual nasal endoscopy browsing experiment.

INDEX TERMS Path planning, robot-assisted endoscopic nasal surgery, surgical robot, virtual nasal endoscopy.

I. INTRODUCTION

In traditional surgery, surgeons usually make surgical plan based on patient's preoperative two-dimensional CT/MRI image sequence. Due to the lack of 3D information, insufficient visualization, and the inability to pre-verify the planned surgical path, the risk and failure rate of surgery is high. With the development of computer technology and image processing technology, computer-aided surgery planning (such as surgical path, incision position, resection range, etc.) has gradually been applied in clinical application, and shows great advantages, such as visible and interactive three-dimensional information in the operation area, and the ability to pre-verify the planned surgical scheme [1]–[4].

Currently, many surgical planning methods and systems have been proposed for computer-aided surgery. From the perspective of surgical planning system, there are mainly stereotactic X-ray planning systems for tumor treatment [5], [6]; automatic positioning planning systems for surgical incisions in laparoscopic surgery [7]–[11]; bone screw implantation and grinding planning systems for orthopedics [12]; surgical planning systems for biopsy and ablation [13]–[15] and surgical planning systems for stomatology [16], [17]. In general, current surgical planning systems varies greatly depending on the type of surgery. In robot-assisted tumor radiotherapy, the focus of surgical planning is how to make the radiotherapy radiation coverage area consistent with the actual tumor shape to reduce unnecessary injury. In robot-assisted laparoscopic surgery, the focus of surgical planning is the incision position and suturing process. In robot-assisted endoscopic nasal surgery, due to the slender and complicated anatomical structure, surgeons are prone to injure surrounding blood vessels, optic nerves and skull base sieve plates during the manipulation

The associate editor coordinating the review of this manuscript and approving it for publication was Gursel Alici.

of surgical instruments [18]–[20]. Therefore, preoperative surgical path planning for safety is a key problem for robot-assisted endoscopic nasal surgery and has important clinical application value.

From the perspective of path planning methods, the current path planning methods mainly include sampling-based methods (such as rapidly exploring random trees, probabilistic road maps), artificial potential field method, grid-based method, etc. Sampling-based method samples the search space, preserves the sample points in free space while removing the sample points in obstacle space, and then constructs the path map and searches for the optimal path from the start point to the target point. Torres et al. successfully implemented the collision-free motion path planning of a concentric tube robot in neurosurgery based on RRT (rapidly exploring random tree) algorithm [21]–[23]. Leibrandt et al. achieved fast and stable path planning of a concentric tube robot based on PRM (probabilistic road maps) algorithm combined with kinematic look-up tables [24]. Park *et al.* [25] used the RRT algorithm to obtain the motion trajectories for a da Vinci surgical robot system, which improved the automation level of the endoscopic camera manipulator and relieved surgeon's workload in surgery. The sampling-based method runs non-exponentially depending on the dimensions of the search space, so they are especially suitable for high-dimensional configuration spaces, but the algorithm cannot determine whether a path exists. Artificial potential field methods generally regard a moving object such as a robot or a car as a point in the search space, which runs under the effect of the attraction force of the target point and the repulsive force of the obstacle. The method is normally solved by gradient descent, and the result is output as a path. In 2014, Li *et al.* [26] proposed a path planning method that uses artificial potential field algorithm together with an improved conjugate gradient algorithm for robot-assisted prostate brachytherapy. In 2017, Liu *et al.* [27] used artificial potential field method to plan collision-free path of intraoperative robot motion in robot-assisted prostate brachytherapy, so as to avoid collision of intraoperative needle tip with surrounding organs. Li *et al.* [13] proposed a discrete potential field algorithm based on 3D anatomical structures to plan the needle path in minimally invasive surgery, such as biopsy and cancer treatment. Experiment result showed that the discrete potential field algorithm can improve targeting accuracy and was beneficial to the therapeutic and diagnostic procedures. The advantage of artificial potential field method is that the amount of calculation is relatively small. However, this method may fall into a local minimum and cannot find a suitable path, or may find a non-optimal path [28], [29]. Grid-based methods generally divide uniform mesh in the search space, and then use search algorithms (such as Dijkstra, A$*$, D$*$) to find the collision-free or optimal path from the starting point to the target point [30]–[32]. In 2016, Granna et al. used grid-based method and wave-front method to plan the blood-sucking path of robot-assisted cerebral hemorrhage surgery. The experiment results showed that the method can effectively shorten the surgical path and improve surgical efficiency [33], [34].

For robot-assisted endoscopic nasal surgical approach planning [35]–[37], considering the narrow and slender surgical operation space, the sampling-based method requires dense sampling points, and there may be cases where the path cannot be found. Also, the artificial potential field method is prone to local extremum problems in the tortuous nasal cavity. Considering that the patient's CT/MRI image sequence can be used to conveniently construct a uniform grid search map, this paper proposes a grid-based method to achieve surgical approach planning, and safe surgical paths from the nasal entrance point to the operating areas are obtained. Firstly, through the stage division of the endoscope movement process, the path planning requirements of the endoscope of robot end-effector in each control stage are analyzed and obtained. Then, considering the slender and complicated anatomy of the nasal cavity, a binarized three-dimensional grid map containing the spatial anatomy of the nasal cavity is constructed based on the patient's CT medical image sequence, and the endoscopic surgical approaches are searched and optimized by introducing the A-star algorithm, safe surgical paths from the nasal entrance point to the operating areas are obtained. Finally, a virtual nasal endoscopy system is developed and tested on a three-dimensional model containing nasal tissue, and the effectiveness of the planned surgical paths is verified by automatic virtual nasal endoscopy browsing experiment.

The remainder of this paper is organized as follows: In section II, the requirements for nasal endoscopic path planning are analyzed. In section III, a binarized three-dimensional grid map containing nasal anatomical structure is constructed based on medical image sequences. The A-star algorithm is adopted to search the safe surgical approaches from the nasal entrance point to the openings of sinuses. In section IV, the virtual nasal endoscopy system is developed to verify the planned endoscopic surgical approaches. The conclusion is summarized in section V.

II. ENDOSCOPIC PATH PLANNING REQUIREMENTS ANALYSIS

Generally, the nasal endoscope tip trajectory of robot end-effector in robot-assisted endoscopic nasal surgery [38]–[41] is shown in Fig. 1.

As can be seen from Fig. 1 that the trajectory of endoscope tip can be divided into three sections:

The first section is from A to B: point A is in the safe area away from the nose of patient, which is the initial position of the endoscope before surgery. When surgery starts, the surgeon drags the end of the robot to point B with free dragging control mode. In this process, because the endoscope tip is far away from the nose of patient, collision is hard to happen. Therefore, it is not necessary to plan the trajectory of the endoscope tip, and the endoscope tip can be directly dragged to the point B.

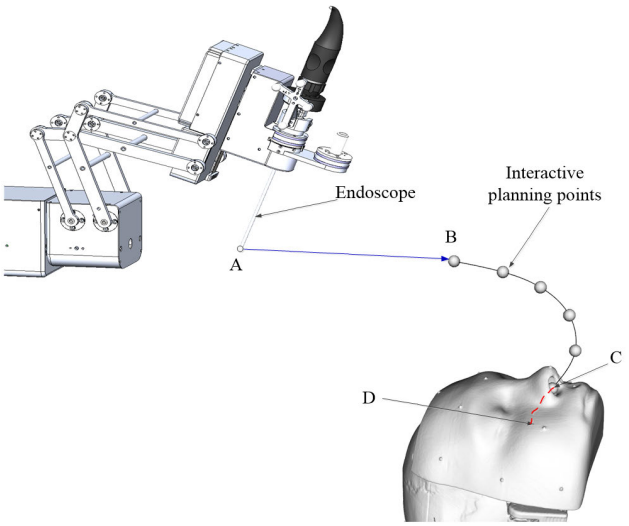

FIGURE 1. The motion trajectory of nasal endoscope tip in robot-assisted endoscopic nasal surgery (taking the right maxillary sinus as an example).

The second section is from B to C: when the endoscope tip of robot end-effector is further dragged from B to C, the endoscope tip is gradually approaching the patient's nostril. To ensure the motion safety during this process and prevent the endoscope tip colliding with the nose of patient, the motion trajectory of the endoscope tip should be planned. In this process, the trajectory of the endoscope is visible. Considering the planning efficiency, the path planning of the endoscope can be performed in human-computer interaction manner. The surgeon interactively edits the cubic polynomial spatial curve in the path planning system (the interactive planning points in Fig. 1), and then the motion path can be adjusted and determined.

The third section is from C to D: when the endoscope tip of robot end-effector is dragged from the point C of the nasal entrance point (near nostril) to the point D of the operation area, such as the opening of right maxillary sinus, the endoscopic tip is inside the nasal cavity of the patient. Due to the slender and complicated anatomical structure of nasal cavity, the endoscope tip is very easy to collide with the nasal tissue during this stage. In order to ensure the safety of surgical operation, the motion path of the endoscope tip must be planned. In this paper, a binarized three-dimensional grid map containing nasal anatomical structure is constructed based on medical image sequences, and then, the A-star algorithm is adopted to search and obtain the path from the point C of the nostril to the point D of the operation area. The details of the proposed path planning method is discussed in Section III.

III. NASAL ENDOSCOPIC SURGICAL APPROACHES PLANNING

A. 3D GRID MAP CONSTRUCTION

To plan the motion path of the endoscope of robot end-effector in the nasal cavity, a three-dimensional map containing nasal anatomical structure must be established.

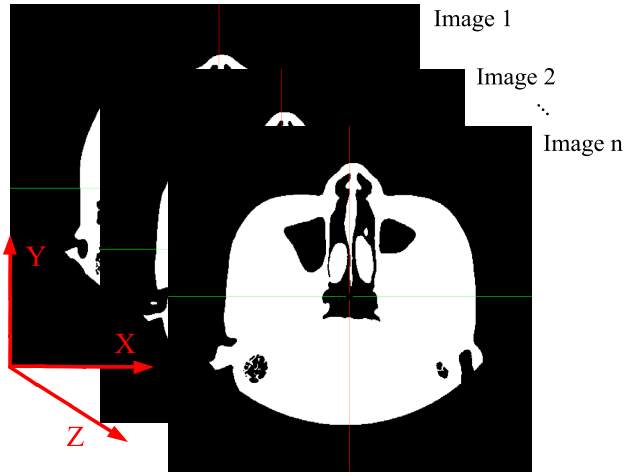

FIGURE 2. Binarized image sequence of patient nasal model.

In this section, based on the patient's CT medical image sequence, through image binarization and spacing processing, a binarized three-dimensional grid-type map with pixels as the basic grid unit is established, which lays a foundation for subsequent path search.

With the Insight Segmentation and Registration Toolkit (ITK), the patient's nasal CT image sequence (DICOM files, a total of 343 images of 512x512 pixels) is read in, and then the patient's nasal cavity and 4 pairs of sinuses (maxillary sinus, ethmoid sinus, sphenoid sinus, and frontal sinus) are threshold segmented and binarized:

$$f(i,j,k) = \begin{cases} 0 & f(i,j,k) < V_{threshold} \\ 255 & f(i,j,k) \geq V_{threshold} \end{cases} \quad (1)$$

The image sequence obtained by binarization is shown in Fig. 2. The image sequence can be used as a uniform grid model of the nasal boundary for subsequent map construction.

Based on the binarized image sequence of nasal model (shown in Fig. 2), a binarized three-dimensional grid-type map is constructed using pixels of the image sequence as basic grid elements: If the pixel gray value is 0, the point is considered to be a free space point; if the pixel gray value is 255, the point is considered as a barrier point; the spatial distance between each grid point is determined by the scan parameters of DICOM image sequence. The final obtained binarized three-dimensional grid map is shown in Fig. 3.

B. PATH SEARCHING ALGORITHM

The current spatial path search methods mainly include best-first search algorithm, Dijkstra's algorithm, A-star algorithm, Sample-based algorithm, etc. In this paper, considering that the patient's CT image sequence can be used to conveniently construct the grid map and the search efficiency, the A-star algorithm is adopted to search the endoscopic path of robot end-effector.

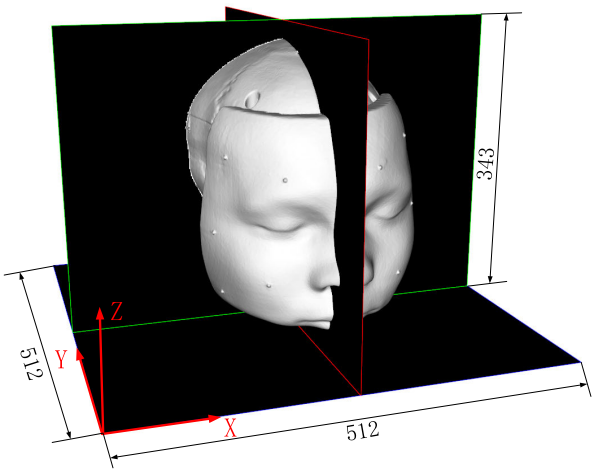

FIGURE 3. Schematic diagram of the binarized three-dimensional grid map.

1) PATH SEARCH ALGORITHM ANALYSIS

The A-star algorithm adds an estimation cost function to change the search direction of the algorithm based on the Dijkstra's algorithm. Therefore, the search efficiency of the A-star algorithm depends largely on the estimation cost function. The more accurate the estimation cost function is constructed, the shorter the search time is and the more accurate the path is. The whole cost function of A-star algorithm is defined as the cost estimation of the least cost path from the starting node through the current node to the target node. In general, the mathematical expression of the whole cost function is as follows:

$$f(n) = g(n) + h(n) \tag{2}$$

where:

$f(n)$- The whole cost function, representing the cost estimation of the least cost path;

$g(n)$ - The known cost function, representing the known cost from the starting node to the current node;

$h(n)$- The estimation cost function, representing the estimated cost from the current node to the target node.

The estimation cost function $h(n)$ is also called a heuristic function. If the map is determined, the value of $h(n)$ is also determined. One key to the A-star algorithm is the precise construction of the heuristic function. In practical applications, it is generally necessary to construct the heuristic function as close as possible to the actual situation. To do this, it is necessary to refer to more heuristic information, however, the amount of calculation will also increase, and therefore the design of this function $h(n)$ needs to be weighed against the actual application.

The commonly used heuristic functions are as follows:

1) The heuristic function based on Manhattan distance: Manhattan distance is a city block distance. The distance between two intersections is calculated according to the sum of the horizontal and vertical differences of the coordinates of the two intersections. Manhattan distance is generally applicable to chessboard maps and block-type maps. For the three-dimensional space, the calculation formula is as follows.

$$h(n) = \text{abs}(x_2 - x_1) + \text{abs}(y_2 - y_1) + \text{abs}(z_2 - z_1) \tag{3}$$

2) The heuristic function based on Chebyshev distance: The distance between two nodes is represented by calculating the maximum value of the coordinate difference between the starting point and the end point. For the three-dimensional space, the calculation formula is as follows.

$$h(n) = \max\left(\text{abs}(x_2 - x_1), \text{abs}(y_2 - y_1), \text{abs}(z_2 - z_1)\right) \tag{4}$$

3) The heuristic function based on Euclidean distance: If an object in a map is allowed to move in any direction, the distance between the two nodes can be expressed by calculating the straight line distance between the starting point and the end point. The calculation formula in the three-dimensional space is as follows.

$$h(n) = sqrt\left((x_2 - x_1)^2 + (y_2 - y_1)^2 + (z_2 - z_1)^2\right) \tag{5}$$

In this paper, considering the endoscope tip can move in any direction, the Euclidean distance is used to construct the heuristic function. At the same time, considering the actual distance between pixels of CT image sequence is generally different, in order to get more precise distance estimation of the actual distance, it is necessary to calculate the path weights in different motion directions. Assuming that the pixel spacing of the CT image sequence in the three directions of X, Y, and Z is δx, δy, δz, the final distance between spatial pixels can be obtained as follows.

$$h(n) = sqrt\left([(x_2 - x_1)\delta x]^2 + [(y_2 - y_1)\delta y]^2 + [(z_2 - z_1)\delta z]^2\right) \tag{6}$$

Assuming that the starting node, the current node, and the target node are respectively $(x_{str}, y_{str}, z_{str})$, $(x_{cur}, y_{cur}, z_{cur})$, $(x_{end}, y_{end}, z_{end})$, the whole cost function formula (2) can be rewritten as:

$$\begin{aligned} f(n) = {} & mindistance[(x_{str}, y_{str}, z_{str}), (x_{cur}, y_{cur}, z_{cur})] \\ & + sqrt\left([(x_{end} - x_{cur})\delta x]^2 + [(y_{end} - y_{cur})\delta y]^2\right. \\ & \left. + [(z_{end} - z_{cur})\delta z]^2\right) \end{aligned} \tag{7}$$

2) PATH PLANNING ALGORITHM PROCESS

Integrating the above algorithm analysis into actual surgery process, the proposed algorithm flow is as follows:

1) Construct a grid map based on the binarized image sequence from patient's CT images. At the same time, the values of F, G, and H in all nodes (F, G and H correspond to the function values of $f(n)$, $g(n)$, $h(n)$ respectively) are set to 0.

2) Initialization: Build and initialize the Open list and the Closed list. Build and initialize the starting node and the target node, calculate the G, H, and F values of the starting node, and then put the starting node into the Open list. Start the path search loop by treating the starting node as the current node.

3) Path search loop:

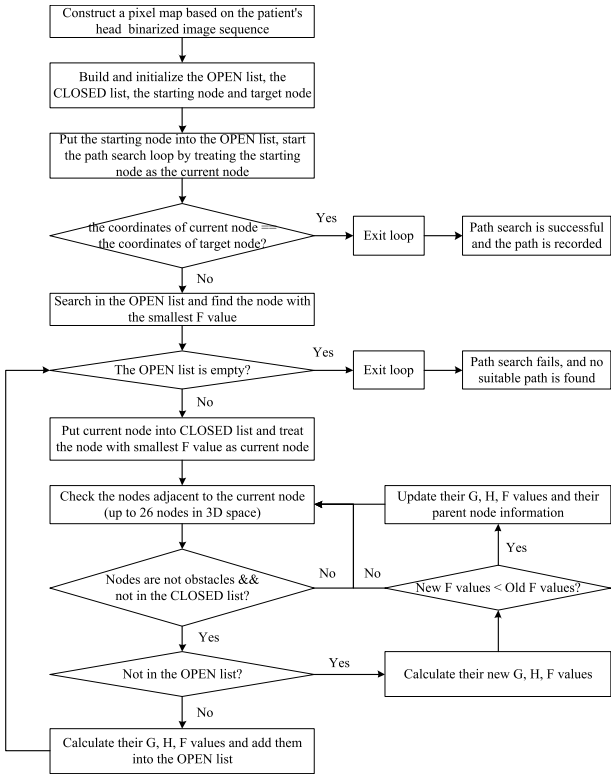

FIGURE 4. Path search algorithm flow chart.

(a) Loop judgment: if the coordinates of current node! = the coordinates of target node;

(b) Search in the Open list and find the node with smallest F value;

(c) If the Open list is empty, exit the loop;

(d) If the Open list is not empty, put the current node into the Closed list and treat the node with smallest F value as the current node;

(e) Check the nodes adjacent to the current node (up to 26 nodes in 3D space): If these nodes are not obstacles, not in the Closed list, not in the Open list; then calculate their G, H, F values and add them into the Open list. If these nodes are not obstacles, not in the Closed list, but in the Open list; then calculate their new G, H, F values. If their new F values are less than the old F values; then update their G, H, F values and their parent node information.

4) After jumping out of the path search loop: If the Open list is empty, the path search fails, and no suitable path is found. If the current node coordinate is equal to the target node coordinate, the path search is successful. The found path can be recorded: starting from the target node, along the parent node information, going back to the starting node to obtain the whole path.

According to the above algorithm flow analysis, the algorithm flow chart can be obtained as shown in Fig. 4.

3) PATH PLANNING ALGORITHM RESULTS

According to the above path planning algorithm analysis, the 3D reconstruction model containing anatomical structure of the nasal cavity is used to interactively specify the starting point (the nasal entrance point, near nostril) and the target point (near the openings of maxillary sinus, ethmoid sinus, sphenoid sinus, and frontal sinus). The motion paths from the nasal entrance point to each sinus opening can be obtained by the proposed search algorithm, as shown in Fig. 5.

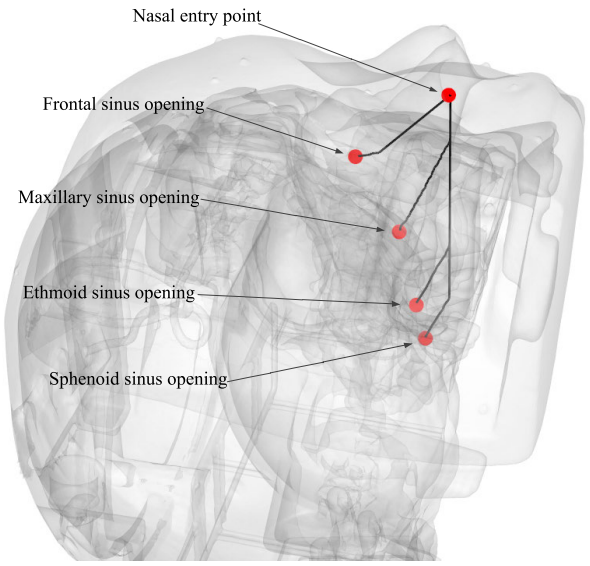

FIGURE 5. Obtained motion paths from the nasal entrance point to the vicinity of each sinus opening.

4) PATH SMOOTHING

Since the path planning algorithm is a pixel by pixel searching process, the obtained path is connected by many straight line segments between pixels. Considering that the planned path is not smooth, and it is not suitable for robot motion control. Therefore, the obtained paths should be smoothed before used in robot control. There are many methods for path smoothing. Considering the convenience of algorithm implementation and the second-order derivative requirement of robot motion trajectory, a Savitzky–Golay filtering method based on local polynomial fitting [42], [43] is adopted to smooth the planned paths.

Assume the window width of the Savitzky-Golay filter is 2N+1, using a k-degree polynomial fit, then

$$y(x) = a_0 + a_1 x + a_2 x^2 + \ldots + a_k x^k \tag{8}$$

For 2N + 1 data points in the window, there are 2N + 1 equations, which constitute the k + 1 element linear equations.

$$\begin{pmatrix} y(x_{-N}) \\ y(x_{-N+1}) \\ \cdots \\ y(x_N) \end{pmatrix} = \begin{pmatrix} 1 & x_{-N} & \ldots & {x_{-N}}^{k-1} & {x_{-N}}^{k} \\ 1 & x_{-N+1} & \ldots & {x_{-N+1}}^{k-1} & {x_{-N+1}}^{k} \\ 1 & \ldots & \ldots & \ldots & \ldots \\ 1 & x_N & \ldots & {x_N}^{k-1} & {x_N}^{k} \end{pmatrix} \begin{pmatrix} a_0 \\ a_1 \\ \ldots \\ a_k \end{pmatrix} \tag{9}$$

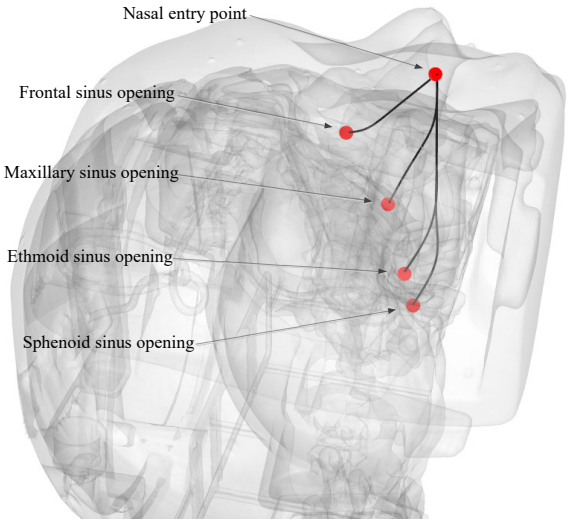

FIGURE 6. Smoothed paths from nose entrance point to the vicinity of each sinus opening.

Assume

$$\mathrm{Y} = \begin{pmatrix} y(x_{-N}) \\ y(x_{-N+1}) \\ \cdots \\ y(x_N) \end{pmatrix} \tag{10}$$

$$\mathrm{X} = \begin{pmatrix} 1 & x_{-N} & \cdots & {x_{-N}}^{k-1} & {x_{-N}}^{k} \\ 1 & x_{-N+1} & \cdots & {x_{-N+1}}^{k-1} & {x_{-N+1}}^{k} \\ 1 & \cdots & \cdots & \cdots & \cdots \\ 1 & x_N & \cdots & {x_N}^{k-1} & {x_N}^{k} \end{pmatrix} \tag{11}$$

$$\mathrm{A} = \begin{pmatrix} a_0 \\ a_1 \\ \cdots \\ a_k \end{pmatrix} \tag{12}$$

Then the least squares method can be used to solve the above equation (9), and the coefficients of the k-degree polynomial can be obtained.

$$\overline{\mathrm{A}} = (\mathrm{X}^{\mathrm{T}}\mathrm{X})^{-1}\mathrm{X}^{\mathrm{T}}\mathrm{Y} \tag{13}$$

The filtered smoothed data points can be obtained as follows.

$$\overline{\mathrm{Y}} = \mathrm{X}(\mathrm{X}^{\mathrm{T}}\mathrm{X})^{-1}\mathrm{X}^{\mathrm{T}}\mathrm{Y} \tag{14}$$

In this paper, through the actual optimization test, the third-order polynomial with a window width of 5 is finally selected for smoothing and filtering, and the smoothed nasal endoscopic motion path is obtained as shown in Fig. 6.

5) PATH COLLISION DETECTION AND INTERACTION OPTIMIZATION

In the previous path planning process, the endoscope tip of robot end-effector is simplified to a pixel point, but in fact the endoscope tip itself has dimensions. In order to prevent the collision between the endoscope tip and the nasal tissue

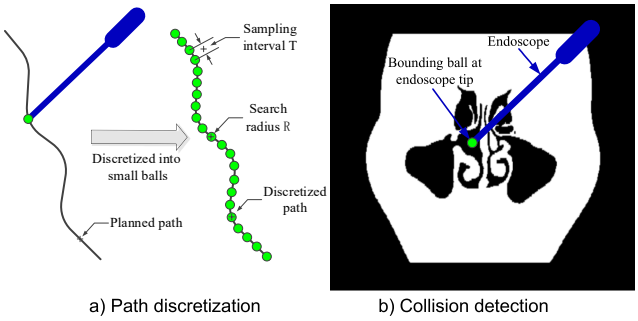

FIGURE 7. Schematic diagram of collision detection based on bounding sphere method between the planned path and the nasal tissue.

during actual movement of robot, it is necessary to consider the diameter of the endoscope, and the collision detection and optimization on the planned motion paths should be performed (the contact between the middle body of endoscope and the nostril is necessary for expanding the surgical operating space in the actual surgery, and the maximum safe contact force is monitored to ensure the safety of contact deformation during surgery. Therefore, path collision detection is only applied between the endoscope tip and the nasal cavity but not the endoscope body inside nasal cavity.).

Discrete sampling is performed on the planned path. Assuming that the diameter of the endoscope is D, the sampling interval is set as T = D/2 (the smaller the sampling interval is, the better the collision detection results, but if the sampling interval is too small, the collision detection efficiency will be lowered). For each sampling point, the bounding sphere method is adopted to detect the collision between the endoscope tip and the nasal tissue. As shown in Fig. 7, the collision detection process is as follows:

1) First of all, the planned path curve is sampled according to the preset sampling interval, so that the planned path is discretized into many uniform small balls centered on the planned path.

2) For any small ball obtained by discretization (the endoscope tip is surrounded by the small ball), assuming that the center position is $P(x, y, z)$, and then the corresponding pixel point of the ball center $Q(i, j, k)$ in the binarized pixel map can be calculated as follows.

$$i = \mathrm{INT}((x - origin.x)/space.x) \tag{15}$$

$$j = \mathrm{INT}((y - origin.y)/space.y) \tag{16}$$

$$k = \mathrm{INT}((z - origin.z)/space.z) \tag{17}$$

where $origin.x$, $origin.y$, and $origin.z$ are the origin coordinates of the pixel map; $space.x$, $space.y$, and $space.z$ are the pixel spacing of the binarized pixel map; and INT() is the rounding function.

3) Assuming the search radius at endoscope tip is R=D/2, the local search range of the collision detection can be calculated as follows:

$$\bar{i} = [-\mathrm{INT}(R/space.x) + i, \mathrm{INT}(R/space.x) + i] \tag{18}$$

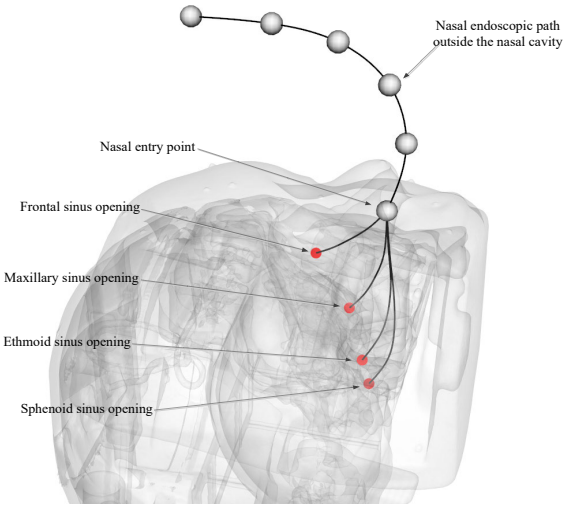

FIGURE 8. The final endoscopic paths from the nasal entrance point to the surgical areas.

$$\bar{j} = [-\mathrm{INT}(R/space.y) + j, \mathrm{INT}(R/space.y) + j] \quad (19)$$

$$\bar{k} = [-\mathrm{INT}(R/space.z) + k, \mathrm{INT}(R/space.z) + k] \quad (20)$$

4) For all pixels in the local search range, the Euclidean distance from each pixel to the endoscope tip (the center of the ball) can be calculated as follows:

$$D = sqrt\left([(\bar{i} - i) \cdot space.x]^2 + [(\bar{j} - j) \cdot space.y]^2 + [(\bar{k} - k) \cdot space.z]^2\right) \quad (21)$$

5) If $Distance < R$ and the pixel gray value is 0 (the pixel gray value is 0, indicating that the pixel is a free space point, and the pixel is shown in black color in Fig. 7), it means that there is no collision. If $Distance < R$ and the pixel gray value is 255 (the pixel gray value is 255, indicating that the pixel is a nasal tissue point, and the pixel is shown in white color in Fig. 7), it means that there is a collision.

The above collision detection method only needs to search for pixel points in the local neighborhood of the nasal endoscope tip, which greatly reduces the calculation amount of the collision detection and improving the detection efficiency.

Since the surface of human nasal cavity is usually covered with a thin mucous, considering the operation safety of surgery, the interference points found in the collision detection need to be adjusted and optimized, and then the collision detection should be performed again to determine the final surgical paths. There are many methods to adjust the path, but considering that the surgeon should do the final decision on the planned path and only fine tuning of the path is required after collision detection, therefore, the human-computer interaction adjusting method through VTK toolkit is adopted in this paper. The vtkSplineWidget in VTK toolkit is used to provide an interactive interface that allows surgeons to easily modify and adjust the planned path, such as interactively adjusting the collision points on the planned path to obtain the final planned path.

Through the above path planning method and subsequent path smoothing, collision detection and interactive path adjustment, the nasal endoscopic motion paths from the nasal entrance point to the surgical areas (near the openings of the maxillary sinus, ethmoid sinus, sphenoid sinus, and frontal sinus) are finally obtained. Fig. 8 shows the final obtained endoscopic paths. Path outside the nasal cavity is generated interactively by surgeons through the path planning system.

IV. EXPERIMENTAL VERIFICATION OF PLANNED ENDOSCOPIC PATHS

For the planned endoscopic paths, if pre-verification can be performed, it is possible to find out whether there is a problem with the planned endoscopic paths in advance, thereby reducing surgical risks and improving the quality of surgery. This section will verify the feasibility of the planned endoscopic paths by constructing a virtual nasal endoscopy system. At the same time, the virtual nasal endoscopy system enables surgeons to more intuitively understand the three-dimensional anatomical information of operation area before surgery and helps to improve the quality of surgery [44].

A. VIRTUAL NASAL ENDOSCOPY SYSTEM DESIGN

The virtual nasal endoscopy system of this paper is based on the previous acquired CT images. The implementation process of the virtual nasal endoscopy system is as follows:

1) Obtain a two-dimensional medical image sequences (generally DICOM format) of the surgical area using a medical imaging device (CT, MRI, etc.);

2) Perform necessary preprocessing on medical image sequences: image filtering, image enhancement, image segmentation, etc.;

3) Perform 3D reconstruction and visualization on the pre-processed image sequences using the surface rendering method;

4) Perform browsing path planning based on the pre-processed image sequences to obtain browsing paths (surgical approaches);

5) Set appropriate virtual nasal endoscopy parameters according to the characteristics of the browsing surgical areas;

6) Design and implement appropriate human-computer interaction styles: human-computer interaction browsing, automatic browsing, etc.

Through the above construction process, a virtual nasal endoscopy system is implemented with VTK toolkit and the system interface is shown in Fig. 9. It mainly includes planned paths management module, paths loading and initialization module, endoscope camera parameters management module, automatic browsing and interactive browsing module. Through the horizontal scroll bar below the image display interface, it can be conveniently adjusted to any point of the planned path for fixed-point observing.

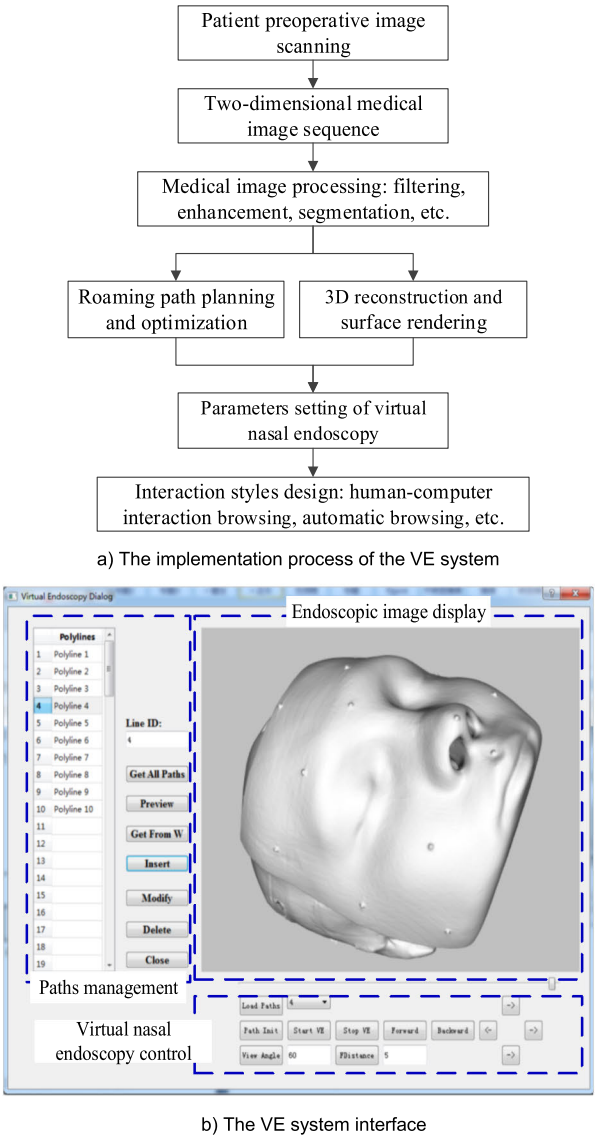

FIGURE 9. The implementation process and interface of virtual nasal endoscopy system.

B. EXPERIMENTAL VERIFICATION OF PLANNED ENDOSCOPIC PATHS

The virtual endoscopy system can be used to simulate the real movement of the nasal endoscope, while displaying the image of the virtual nasal endoscopy in real time. Therefore, it can be conveniently used to pre-verify the planned surgical paths.

The virtual nasal endoscopy systems have two operation modes: an automatic browsing mode and an interactive browsing mode. In the automatic browsing mode, the surgeon selects the planned paths on the left side of the interface, sets the angle of view and focal length, and then clicks the Start VE button. The virtual nasal endoscope will automatically browse along the selected path, and the right interface will display the virtual image of the endoscope in real time. In the interactive browsing mode, the surgeon can select the points of interest on the planned path for multi-angle observation and can also move the points of interest interactively up and down (the button at the lower right corner of the interface). In this mode, the surgeon can conveniently select the observing area and angle, and observe some areas that traditional endoscope cannot observe.

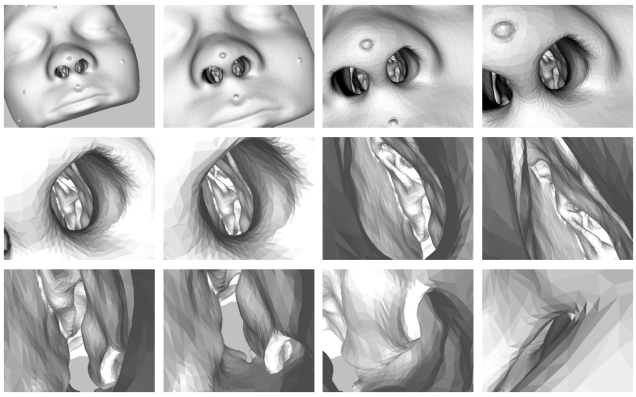

FIGURE 10. Snapshots during the automatic browsing.

In this paper, the automatic browsing mode is adopted with the planned path as a pathway. The virtual nasal endoscope automatically moves along the planned path while acquiring images in real time. By observing the image quality during the virtual nasal endoscopy, it is judged whether the planned path interferes with the nasal tissue, and whether the surgical field of view changes smoothly, thereby verifying the feasibility of the planned paths.

Fig. 10 shows part of virtual endoscopic images acquired during the automatic browsing.

It can be seen from Fig. 10 that based on the virtual nasal endoscopy system, the rationality and safety of the planned surgical paths can be verified with the automatic browsing mode. At the same time, the surgeon can more intuitively understand the three-dimensional anatomy of the operation area before surgery, which helps to improve the quality of surgery.

V. CONCLUSION

In order to improve the motion safety of nasal endoscope in robot-assisted endoscopic nasal surgery, a path planning method of endoscopic surgical approaches based on medical image pixel map search was proposed, and safe surgical paths from the nasal entrance point to the operating areas were obtained. Firstly, through the nasal endoscope tip trajectory analysis during surgery, the motion trajectory of endoscope tip had been divided into three stages. For each stage, the characteristics of trajectory were analyzed and the corresponding path planning requirements of endoscope tip were obtained. Then, considering that the patient's image sequence can conveniently construct a grid-type map, a three-dimensional map containing the spatial anatomy of nasal cavity was constructed by threshold segmentation, binarization and pixel spacing processing of the patient's image sequence. Through analyzing the estimation cost function of A-star path search algorithm, the optimal path cost estimation method close to the actual situation was obtained by using the

Euclidean distance calculation, and the endoscopic surgical approaches were searched and smoothed. Considering the diameter of the endoscope tip, the collision detection and interactive optimization on the planned motion paths were performed, and safe surgical paths from the nasal entrance point to each sinus opening were obtained. Finally, to verify the planned endoscopic paths before surgery, a virtual nasal endoscopy system was developed and tested on a head model containing nasal tissue, and the effectiveness of the planned surgical paths was verified by automatic virtual nasal endoscopy browsing experiment. In future, the proposed path planning method will be evaluated on high fidelity head models and cadaver heads. What needs to be focused on is the effect of the deformation of nasal tissue on the planning path.

REFERENCES

[1] A. Austad, O. Elle, and J. Røtnes, "Computer-aided planning of trocar placement and robot settings in robot-assisted surgery," *Int. Congr. Ser.*, vol. 1230, pp. 1020–1026, Jun. 2001.

[2] R. Bauernschmitt, M. Feuerstein, J. Traub, E. U. Schirmbeck, G. Klinker, and R. Lange, "Optimal port placement and enhanced guidance in robotically assisted cardiac surgery," *Surgical Endoscopy*, vol. 21, no. 4, pp. 684–687, Mar. 2007.

[3] W. Wang, W. Wang, W. Dong, Z. Du, and Y. Sun, "A preoperative planning algorithm based on dexterity and collaboration space for the robot-assisted minimally invasive surgery," *Robot*, vol. 38, pp. 208–216, Mar. 2016.

[4] J. Yang, L. Yu, L. Wang, Z. Tang, and Y. Li, "Preoperative planning of a celiac minimally invasive surgery robot based on feature parameters and double collaboration space," *Robot*, vol. 39, pp. 230–238, Feb. 2017.

[5] R. Z. Tombropoulos, J. R. Adler, and J.-C. Latombe, "CARABEAMER: A treatment planner for a robotic radiosurgical system with general kinematics," *Med. Image Anal.*, vol. 3, no. 3, pp. 237–264, Sep. 1999.

[6] A. Schweikard, R. Tombropoulos, L. Kavraki, J. Adler, and J.-C. Latombe, "Treatment planning for a radiosurgical system with general kinematics," in *Proc. IEEE Int. Conf. Robot. Autom.*, Dec. 2002, pp. 1720–1727.

[7] J. Cannon, J. Stoll, S. Selha, P. Dupont, R. Howe, and D. Torchiana, "Port placement planning in robot-assisted coronary artery bypass," *IEEE Trans. Robot. Autom.*, vol. 19, no. 5, pp. 912–917, Oct. 2003.

[8] È. Coste-Manière, L. Adhami, F. Mourgues, and O. Bantiche, "Optimal planning of robotically assisted heart surgery: First results on the transfer precision in the operating room," *Int. J. Robot. Res.*, vol. 23, nos. 4–5, pp. 539–548, Apr. 2004.

[9] L. Adhami, È. Coste-Manière, and J.-D. Boissonnat, "Planning and simulation of robotically assisted minimal invasive surgery," in *Proc. Int. Conf. Med. Image Comput. Comput.-Assist. Intervent*, 2000, pp. 624–633.

[10] Y. Wang, "Structural analysis and preoperative planning virtual modeling and simulation of abdominal minimally invasive surgery robot," M.S. thesis, Tianjin Univ., Tianjin, China, 2009.

[11] R. Konietschke, H. Weiss, T. Ortmaier, and G. Hirzinger, "A preoperative planning procedure for robotically assisted minimally invasive interventions," in *Proc. 3rd Conf. German Soc. Comput. Robotic Assist. Surg. (CURAC)*, 2004, pp. 1–8.

[12] X. Zheng, "Compliance control and bone grinding surgery planning for spinal surgery robot," Hunan Univ., Changsha, China, 2013.

[13] P. Li, S. Jiang, D. Liang, Z. Yang, Y. Yu, and W. Wang, "Modeling of path planning and needle steering with path tracking in anatomical soft tissues for minimally invasive surgery," *Med. Eng. Phys.*, vol. 41, pp. 35–45, Mar. 2017.

[14] G. J. Vrooijink, M. Abayazid, S. Patil, R. Alterovitz, and S. Misra, "Needle path planning and steering in a three-dimensional non-static environment using two-dimensional ultrasound images," *Int. J. Robot. Res.*, vol. 33, no. 10, pp. 1361–1374, Sep. 2014.

[15] F. Liu, A. Garriga-Casanovas, R. Secoli, and F. Rodriguez Y Baena, "Fast and adaptive fractal tree-based path planning for programmable bevel tip steerable needles," *IEEE Robot. Autom. Lett.*, vol. 1, no. 2, pp. 601–608, Jul. 2016.

[16] J. Jiang, Y. Zhang, and W. Zhang, "Collaborative simulation and experimentation on the dental arch generator of a multi-manipulator tooth-arrangement robot," *Int. J. Adv. Robot. Syst.*, vol. 9, no. 2, p. 43, Aug. 2012.

[17] A. S. K. Salamah and M. S. Drogomyretska, "A glance about the applications of robot in orthodontics," *Int. J. Innov. Sci. Res.*, vol. 12, pp. 178–182, 2016.

[18] R. Slack and G. Bates, *Functional Endoscopic Sinus Surgery*, vol. 58. American Family Physician, Leawood, KS, USA, 1998, pp. 707–720.

[19] H. Khalil and D. A. Nunez, "Functional endoscopic sinus surgery for chronic rhinosinusitis," in *Cochrane Database of Systematic Reviews*. Chichester, U.K.: Wiley, 2006.

[20] B. A. Senior, D. W. Kennedy, J. Tanabodee, H. Kroger, M. Hassab, and D. Lanza, "Long-term results of functional endoscopic sinus surgery," *Laryngoscope*, vol. 108, pp. 151–157, Feb. 1998.

[21] L. G. Torres, C. Baykal, and R. Alterovitz, "Interactive-rate motion planning for concentric tube robots," in *Proc. IEEE Int. Conf. Robot. Autom. (ICRA)*, May 2014, pp. 1915–1921.

[22] L. G. Torres and R. Alterovitz, "Motion planning for concentric tube robots using mechanics-based models," in *Proc. IEEE/RSJ Int. Conf. Intell. Robots Syst.*, Sep. 2011, pp. 5153–5159.

[23] L. G. Torres, A. Kuntz, H. B. Gilbert, P. J. Swaney, R. J. Hendrick, R. J. Webster, and R. Alterovitz, "A motion planning approach to automatic obstacle avoidance during concentric tube robot teleoperation," in *Proc. IEEE Int. Conf. Robot. Autom. (ICRA)*, May 2015, pp. 2361–2367.

[24] K. Leibrandt, C. Bergeles, and G.-Z. Yang, "Concentric tube robots: Rapid, stable path-planning and guidance for surgical use," *IEEE Robot. Autom. Mag.*, vol. 24, no. 2, pp. 42–53, Jun. 2017.

[25] J.-H. Park, W. J. Park, C. Lee, M. Kim, S. Kim, and H. J. Kim, "Endoscopic camera manipulation planning of a surgical robot using rapidly-exploring random tree algorithm," in *Proc. 15th Int. Conf. Control, Autom. Syst. (ICCAS)*, Oct. 2015, pp. 1516–1519.

[26] P. Li, S. Jiang, J. Yang, and Z. Yang, "A combination method of artificial potential field and improved conjugate gradient for trajectory planning for needle insertion into soft tissue," *J. Med. Biol. Eng.*, vol. 34, pp. 568–573, 2014.

[27] F. Liu, Z.-Y. Yang, S. Jiang, P. Li, and D. Liang, "3D trajectory planning algorithm for organ groups and irregular obstacles with application for prostate brachytherapy," in *Proc. 13th IEEE Conf. Autom. Sci. Eng. (CASE)*, Aug. 2017, pp. 1420–1424.

[28] O. Khatib, "Real-time obstacle avoidance for manipulators and mobile robots," in *Proc. IEEE Int. Conf. Robot. Automat.*, Mar. 1985, pp. 500–505.

[29] B. F. Zhang, Y. C. Wang, and X. L. Zhang, "Mobile robot path planning based on artificial potential field method," *Appl. Mech. Mater.*, vol. 577, pp. 350–353, Jul. 2014.

[30] S. Wong and B. Macdonald, "A topological coverage algorithm for mobile robots," in *Proc. IEEE/RSJ Int. Conf. Intell. Robots Syst. (IROS)*, Apr. 2004, pp. 1685–1690.

[31] Y. Gabriely and E. Rimon, "Competitive on-line coverage of grid environments by a mobile robot," *Comput. Geometry*, vol. 24, no. 3, pp. 197–224, Apr. 2003.

[32] E. Galceran and M. Carreras, "A survey on coverage path planning for robotics," *Robot. Auto. Syst.*, vol. 61, no. 12, pp. 1258–1276, Dec. 2013.

[33] J. Granna, I. S. Godage, R. Wirz, K. D. Weaver, R. J. Webster, and J. Burgner-Kahrs, "A 3-D volume coverage path planning algorithm with application to intracerebral hemorrhage evacuation," *IEEE Robot. Autom. Lett.*, vol. 1, no. 2, pp. 876–883, Jul. 2016.

[34] J. Granna, Y. Guo, K. D. Weaver, and J. Burgner-Kahrs, "Comparison of optimization algorithms for a tubular aspiration robot for maximum coverage in intracerebral hemorrhage evacuation," *J. Med. Robot. Res.*, vol. 2, 2017, Art. no. 1750004.

[35] M. Rilk, F. M. Wahl, K. W. Eichhorn, I. Wagner, and F. Bootz, "Path planning for robot-guided endoscopes in deformable environments," in *Advances in Robotics Research*. Berlin, Germany: Springer, 2009, pp. 263–274.

[36] M. Li and R. Taylor, "Performance of surgical robots with automatically generated spatial virtual fixtures," in *Proc. IEEE Int. Conf. Robot. Autom.*, Jan. 2006, pp. 217–222.

[37] M. Li, *Intelligent Robotic Surgical Assistance for Sinus Surgery*. Baltimore, MD, USA: Johns Hopkins Univ., 2006.

[38] Y. He, B. Zhao, X. Hou, P. Gao, Y. Hu, and P. Zhang, "An assistant robot system for sinus surgery," *J. Med. Devices*, vol. 10, Sep. 2016, Art. no. 30925.

[39] Y. He, Y. Hu, P. Zhang, B. Zhao, X. Qi, and J. Zhang, "Human–robot cooperative control based on virtual fixture in robot-assisted endoscopic sinus surgery," *Appl. Sci.*, vol. 9, no. 8, p. 1659, Apr. 2019.

[40] Q. Zheng, Y. He, X. Qi, P. Zhang, Y. Hu, and B. Li, "Safety tracking motion control based on forbidden virtual fixtures in robot assisted nasal surgery," *IEEE Access*, vol. 6, pp. 44905–44916, 2018.
[41] Y. He, *Research on Mechanism Design and Safety Control of Endoscopic Sinus Surgery Assisatant Robot*. Beijing, China: Univ. of Chinese Academy of Sciences, 2019.
[42] B. Wang, "The filtering technique of gas logging curve based on savitzky-golay algorithm," *West-China Explor. Eng.*, vol. 29, pp. 30–31, 2017.
[43] A. Savitzky and M. J. E. Golay, "Smoothing and differentiation of data by simplified least squares procedures." *Anal. Chem.*, vol. 36, no. 8, pp. 1627–1639, Jul. 1964.
[44] X. Gao, L. Tian, L. Wang, and Z. Mao, "Key technique analysis of virtual endoscopy," *Appl. Res. Comput.*, vol. 25, pp. 1956–1959, Jul. 2008.

YUCHENG HE received the B.S. degree from Southeast University, Nanjing, China, in 2004, the M.S. degree from Xi'an Jiaotong University, Xi'an, China, in 2007, and the Ph.D. degree from the University of Chinese Academy of Sciences, Beijing, China, in 2019.

He is currently a Research Assistant with the Center for Cognitive Technology, Shenzhen Institute of Advanced Technology, Chinese Academy of Sciences, China. His current research interests include surgical robots and medical automation equipment.

PENG ZHANG received the B.S. degree from Jilin University, in 2003, and the M.S. and Ph.D. degrees from the School of Mechatronics Engineering, Harbin Institute of Technology, in 2005 and 2010, respectively.

He is currently a Senior Engineer with the Center for Cognitive Technology, Shenzhen Institute of Advanced Technology, Chinese Academy of Sciences, China. His current research interests include medical/surgical robots, medical automation equipment, and virtual simulation technology.

XIAOZHI QI received the B.S. degree from Yanshan University, in 2009, and the M.S. and Ph.D. degrees from the Harbin Institute of Technology at Shenzhen, China, in 2011 and 2017, respectively.

He currently holds a postdoctoral position with the University of Hamburg, Germany, and also an Associate Professor with the Shenzhen Institutes of Advanced Technology, Chinese Academy of Sciences, China. His research interests include medical assistant robots and space deployable mechanisms.

BAOLIANG ZHAO received the B.S. degree from Yanshan University, Qinhuangdao, China, in 2008, the M.S. degree from Tongji University, Shanghai, China, in 2011, and the Ph.D. degree in mechanical engineering from the University of Nebraska–Lincoln, Lincoln, USA, in 2015.

He is currently a Senior Engineer with the Center for Cognitive Technology, Shenzhen Institute of Advanced Technology, Chinese Academy of Sciences, China. His research interests include medical robots, mobile robots, and automation.

SHIBO LI received the B.S. and M.S. degrees from Beihang University, in 2009 and 2012, respectively, and the Ph.D. degree from the University of Alabama, USA, in 2016.

He currently holds a postdoctoral position with the Shenzhen Institutes of Advanced Technology, Chinese Academy of Sciences, China. His research interests include medical assistant robots, biomechanics, and composite mechanics.

YING HU (Member, IEEE) received the B.S. degree from Shanghai Jiao Tong University, Shanghai, China, in 1996, and the M.S. and Ph.D. degrees in mechanical engineering from the Harbin Institute of Technology, Shenzhen, China, in 1998 and 2007, respectively.

She is currently a Professor with the Center for Cognitive Technology, Shenzhen Institute of Advanced Technology, Chinese Academy of Sciences, China. She has authored or coauthored more than 60 scientific articles published in refereed journals and conference proceedings. Her research interests include parallel robots, medical assistant robots, and mobile robots.